JOURNAL OF GEOPHYSICAL RESEARCH, VOL. 95, NO. B4, PAGES 4763–4776, APRIL 10, 1990

Tomographic Imaging of Local Earthquake Delay Times for Three-Dimensional Velocity Variation in Western Washington

JONATHAN M. LEES[1] AND ROBERT S. CROSSON

Geophysics Program, University of Washington

Tomographic inversion is applied to delay times from local earthquakes to image three dimensional velocity variations in the Puget Sound region of Western Washington. The 37,500 square km region is represented by nearly cubic blocks of 5 km per side. P-wave arrival time observations from 4,387 crustal earthquakes, with depths of 0 to 40 km, were used as sources producing 36,865 rays covering the target region. A conjugate gradient method (LSQR) is used to invert the large, sparse system of equations. To diminish the effects of noisy data, the Laplacian is constrained to be zero within horizontal layers, providing smoothing of the model. The resolution is estimated by calculating impulse responses at blocks of interest and estimates of standard errors are calculated by the jackknife statistical procedure. Results of the inversion are correlated with some known geologic features and independent geophysical measurements. High P-wave velocities along the eastern flank of the Olympic Peninsula are interpreted to reflect the subsurface extension of Crescent terrane. Low velocities beneath the Puget Sound further to the east are inferred to reflect thick sediment accumulations. The Crescent terrane appears to extend beneath Puget Sound, consistent with its interpretation as a major accretionary unit. In the southern Puget Sound basin, high velocity anomalies at depths of 10-20 km are interpreted as Crescent terrane and are correlated with a region of low seismicity. Near Mt. Rainier, high velocity anomalies may reflect buried plutons.

INTRODUCTION

The extensive seismicity in the crust and upper mantle of the Puget Sound basin has been the focus of study since the early 1970's when the western Washington seismic network was initially established. While seismicity patterns have been used to infer structural faults and tectonics in the region [e.g. *Weaver and Smith*, 1983], the location of hypocenters is a function of one's knowledge of the seismic velocity structure of the region. A three dimensional, laterally heterogeneous P-wave velocity model should allow improved hypocenter locations while at the same time providing additional insight into the structures controlling the tectonics. The goal of this research is to produce such a three-dimensional velocity model by applying tomographic imaging techniques to travel time observations from local earthquakes. The resultant model has large and small scale features which correlate with independent geophysical measurements, lending validity to the tomographic method and strengthening inferences made from those observations. Furthermore, our results may contribute to a better understanding of the complex nature of lithospheric accretion in this region. Imaging of the geologic structures in the subsurface should also lead to a better understanding of the spatial distribution of seismicity and seismic hazards.

Since the early Cretaceous, the tectonics of western Washington has been dominated by convergence of the Farallon plate with the North American plate. The general nature of the convergence of these plates was described by *Atwater* [1970] and *Armstrong* [1978] and details of the convergence related to the Tertiary accretions to the North American craton are outlined in *Duncan* [1982] and *Wells et al.* [1984]. The features relevant to this study can be divided into four major tectonic units starting from the east working westward: 1) pre-Tertiary sedimentary and volcanic rocks and Quaternary volcanics overlying Precambrian to Mesozoic basement on the western flank of the Cascade range, 2) Mesozoic marine sedimentary and basaltic rocks in central Puget Sound overlain by thick glacial deposits, 3) lower Eocene basalts of the Crescent terrane in Washington and the Metchosin on Vancouver Island which have surface exposure on the eastern flanks of the Olympic Mountains and extend southward into Oregon, 4) the Core rocks of the Olympic Peninsula, comprising Cenozoic marine sediments [*Clowes et al.*, 1987; *Johnson*, 1984; *Taber*, 1983].

A detailed discussion of the evolution of the Cascade volcanic system was provided by *McBirney* [1978]. Extensive volcanism began during the second half of the Mesozoic and has been continuing episodically to the present. Major spurts of intense activity are known to have occurred in late Eocene to early Miocene, mid- to late Miocene, Pliocene and in the Quaternary. The present active volcanism began approximately 1 million years ago. Basalt flows from fissures as well as plutonic bodies are present along the Cascades from Canada to Oregon [*McBirney*, 1978]. Several plutons are exposed near Mt. Rainier [*Cowan and Potter*, 1986; *Walsh et. al.*, 1987] and Mt. St. Helens [*Evarts et al.*, 1987]. The Tertiary volcanic sediments are believed to overlay Precambrian to Mesozoic basement which is exposed in northern Washington and Canada [*Clowes et al.*, 1987]. On the west flank of the Cascades there are several exposed sedimentary basins, particularly the Chuckanut Formation to the north and the Puget Group to the southeast of Puget Sound. These are predominantly nonmarine Eocene sediments [*Johnson*, 1984].

The Puget Sound basin is largely covered by a thick layer of glaciated sediments in some places reaching to depths of 6 km [*Hall and Othberg*, 1974]]. Below this extensive region of

[1]Now at Institute for Crustal Studies, University of California, Santa Barbara.

Paper number 90JB00263.
0148-0227/90/90JB-00263$05.00

unconsolidated sediments, it is believed there is a thick (up to 20 km thick) accretionary package of sedimentary rocks of submarine origin [*MacQueen*, 1982; *Clowes et al.*, 1987]. Because of the thickness of the Quaternary sediments little is known from surface exposure about the geology at depth.

The east flank of the Olympic Mountains is dominated by a unit of Eocene basalts, known as the Crescent formation in Washington, which is correlated to the Metchosin formation of southern Vancouver Island [*Clowes et al.*, 1987]. This formation is a linear feature along the northwest Pacific coast from Canada to central Oregon, and has been the subject of several recent investigations [*Taber and Smith*, 1985; *Duncan*, 1982; *Wells et al.*, 1984]. *Duncan* [1982] interpreted these rocks as seamounts which were subsequently accreted against the North American plate. *Johnson* [1984] suggests that a major transcurrent fault system borders the Crescent formation in southern Vancouver Island and trends southward, perhaps under Puget Sound.

The central Olympic Mountains largely comprise a unit of sedimentary rocks called the Core rocks by *Tabor and Cady* [1978]. These rocks, emplaced after the Crescent, extend to the continental shelf adjacent to Vancouver Island and Washington [*Clowes et al.*, 1987]. The eastern Core rocks, emplaced next to the Crescent terrane, are more deformed than those lying to the west [*Tabor and Cady*, 1978], indicating extensive compression during accretion.

Geophysical studies conducted in western Washington include gravity, seismic, aeromagnetic and electrical conductivity measurements. A complete Bouguer gravity anomaly map was published by *Bonini et al.* [1974] which shows a gravity ridge that coincides with the Crescent rocks on the eastern flank of the Olympic uplift. In the Puget Sound

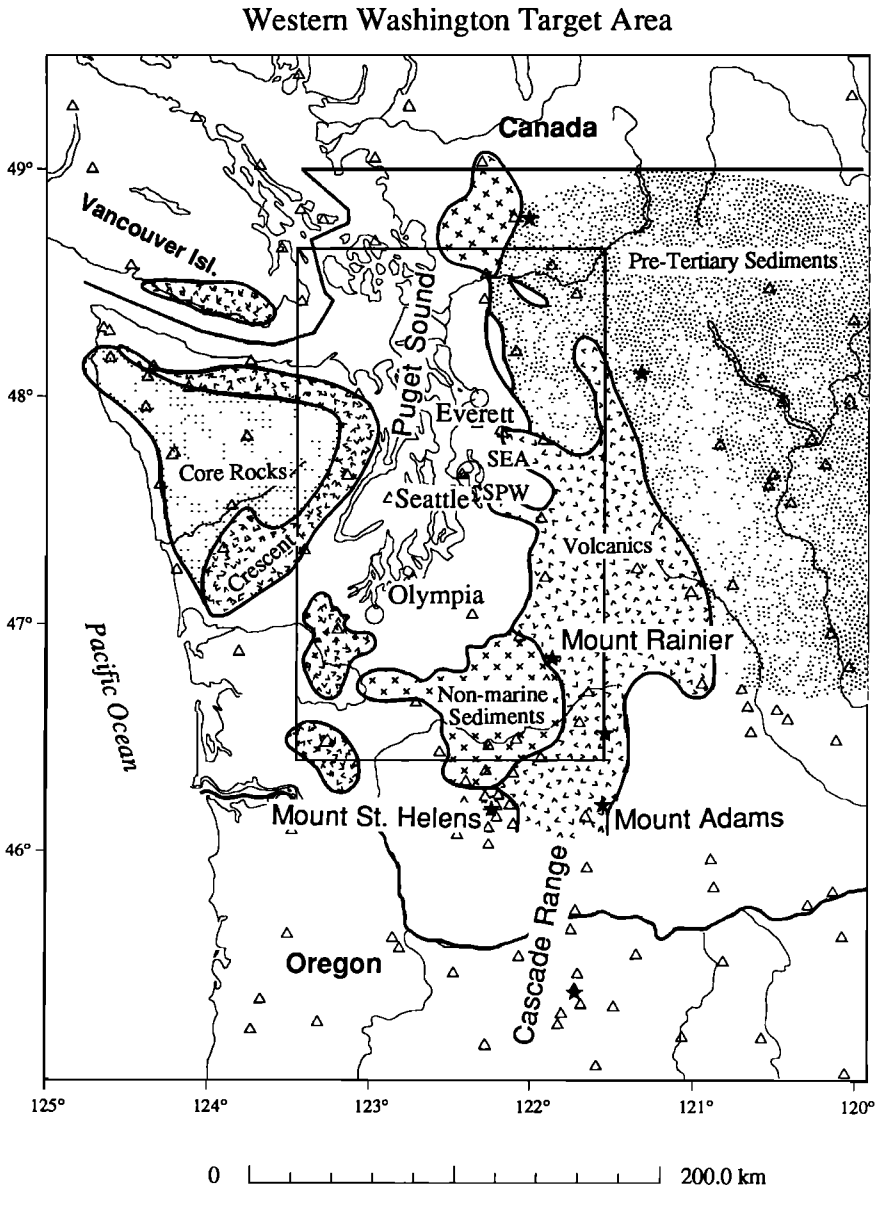

Fig. 1. Map of target areas and station distribution of the western Washington seismic network. Triangles are station locations and stars are major strato-volcanos in the Cascade range. Important geological features discussed in the text, such as the Crescent formation and the Core rocks in the Olympic Peninsula, are indicated. The Puget Sound lowland lies between the Olympic Mountains to the west and the Cascade range to the east. Stations SEA and SPW are labelled for reference.

basin, three major gravity lows are present: southeast of Olympia, over Lake Washington in Seattle and in the Everett region. A steep gravity gradient trends south on the western border of the Puget Sound and takes a sharp bend to the southeast near of Olympia. *Gower et al.* [1985] have interpreted these large gravity gradients as being evidence for faults below the unconsolidated sediments. Seismicity in the Puget Sound is generally divided into two zones [*Crosson and Owens*, 1987]: deep seismicity associated with the subduction and shallow (< 40 km), diffuse seismicity distributed mainly in the central to northern Puget Sound region. While some lineations of seismicity are apparent, there are no known faults that coincide with specific alignments of shallow earthquakes [*Gower et al.*, 1985]. Reflection and refraction studies have been used on southern Vancouver Island to help define the accretionary geometry of the underthrusting terranes [*Clowes et al.*, 1987]. High impedance contrasts were observed at boundaries between the Crescent and adjacent marine sedimentary wedges. *Taber and Lewis* [1986] interpreted onshore-offshore refraction data obtained west of our study area for general crust and upper mantle structure. Electrical conductivity anomalies in the region roughly bounded by Mt. Rainier, Mt. St. Helens and Mt. Adams have been interpreted by *Stanley et al.* [1987] to be evidence for marine forearc basin sediments accreted to North America during the Eocene. Several aeromagnetic surveys have been performed over parts of western Washington [*Manson*, 1984] and are discussed by *Stanley et al.* [1987] and *Finn and Williams* [1987]. Broad high aeromagnetic anomalies are present in the south end of the Puget Sound and southwest of Mt. St. Helens [*Stanley et al.*,1987].

DATA

The target region for the Puget Sound inversion is shown in Figure 1 along with the western Washington seismic network stations represented as triangles. Major strato-volcanos are designated on the map by stars, and stations SPW and SEA are labeled for further reference. The lateral dimensions of the target are 150 km in the east-west direction and 250 km north-south ranging from 46.4° to 48.65° latitude north and 121.47° to 123.42° longitude west. This target was chosen primarily for its concentration of seismicity. The target area was divided laterally into blocks 5 km square and 10 layers to a depth of 41 km according to the reference model described in Table 1. This implies an inversion with a maximum of 16,000 blocks, however only 10,554 blocks were actually sampled by rays from the selected data. In the center of the model, below 6 km depth, several blocks were sampled by more than 500 rays.

Earthquakes were chosen from the western Washington seismic network data-base including data from 1972 to 1988. Earthquakes located within the target volume were selected by the following additional criteria: 1) azimuthal gap ≤ 180° (median = 110°); 2) number of stations ≥ 5; 3) minimum distance ≤ 50 km (median = 15 km); 4) RMS residual ≤.5 sec; and 5) magnitude ≥ 0.0. From this data set, only those rays (station-hypocenter pairs) that remained entirely within the target volume were used for inversion, thus excluding earthquakes deeper than 40 km. Station corrections were determined by visually estimating time delays from histogram plots of residuals for each station, using all the data in the network (including data outside the target). The time delays were used to remove the effects of near station structure and

Table 1. Puget Sound Velocity Model

Layer	Depth	Reference Velocity	Minimum %Slowness	Maximum %Slowness	Minimum Velocity	Maximum Velocity	-5% Velocity	+5% Velocity
1	0.00	5.40	-11.55	6.24	5.08	6.10	5.14	5.68
2	2.00	5.89	-6.78	9.93	5.36	6.32	5.61	6.20
3	4.00	6.38	-3.98	11.80	5.71	6.64	6.08	6.72
4	6.00	6.46	-7.73	6.58	6.06	7.00	6.15	6.80
5	9.00	6.59	-5.69	4.94	6.28	6.99	6.28	6.94
6	12.00	6.65	-5.74	4.06	6.39	7.06	6.33	7.00
7	16.00	6.73	-4.77	3.39	6.51	7.07	6.41	7.08
8	20.00	6.86	-3.64	6.11	6.47	7.12	6.53	7.22
9	25.00	6.95	-2.44	3.59	6.71	7.12	6.62	7.32
10	32.00	6.90	-0.83	1.02	6.83	6.96	6.57	7.26
11	41.00	7.80	0.00	0.00	7.80	7.80	7.43	8.21

Velocity Model for the Puget Sound. Columns 4 and 5 represent the minimum and maximum percent perturbations for the given layers and columns 6 and 7 are the corresponding velocities for the respective extreme perturbations. Columns 8 and 9 are the velocities for ±5% perturbation anomalies as plotted in Figure 4.

elevation. Determinations of station corrections and hypocenter locations were then iterated until residual distributions at each station were approximately zero mean and symmetric [*Lees and Crosson*, 1989]. After station corrections were determined, hypocenter locations and event times were fixed and assumed known. Rays with residuals greater than 2 seconds were excluded as outliers since nearly 98% of the residuals were less than 1 second. There were 4,387 earthquakes that passed the above criteria resulting in 36,865 raypaths used for the inversion. The epicenters are plotted on a map view of the target area in Figure 2. There is a relatively good distribution except for sparse source coverage in the southwest part of the target area.

An estimate of the picking uncertainty was assigned by the seismic analyst for each arrival time. These estimates were used as weights in the inversion procedure to place heavier emphasis on data with smaller uncertainty. We have also reduced the effect of bias that occurs in heavily sampled parts of the model by down weighting data from raypath clusters [*Humphreys and Clayton*, 1988]. Estimates for the uncertainties in hypocenter locations were not incorporated in the inversion. When the number of model parameters is relatively small and the number of data is not too large, one can invert simultaneously for velocity structure and hypocenter location simultaneously [*Crosson*, 1976; *Thurber*, 1983; *Ishida and Hasemi*, 1988]. However, the use of over 4000 earthquakes and over 10,000 model parameters requires the implementation of sparse matrix techniques. Since the addition of hypocenter locations as parameters results in denser matrices which are not as suitable for sparse techniques, we chose not to pursue this approach for this analysis. Nearly all the velocity anomalies found in this study were less than 8% suggesting that the assumptions of linearity are not inappropriate. The calculation of a non-linear inverse may be attained by recalculating raypaths and hypocenter locations using the first-order perturbed model and then iterating towards convergence. This step was not attempted primarily because of the inordinate amount of time required for three-dimensional raypath calculations with such a large model and data set.

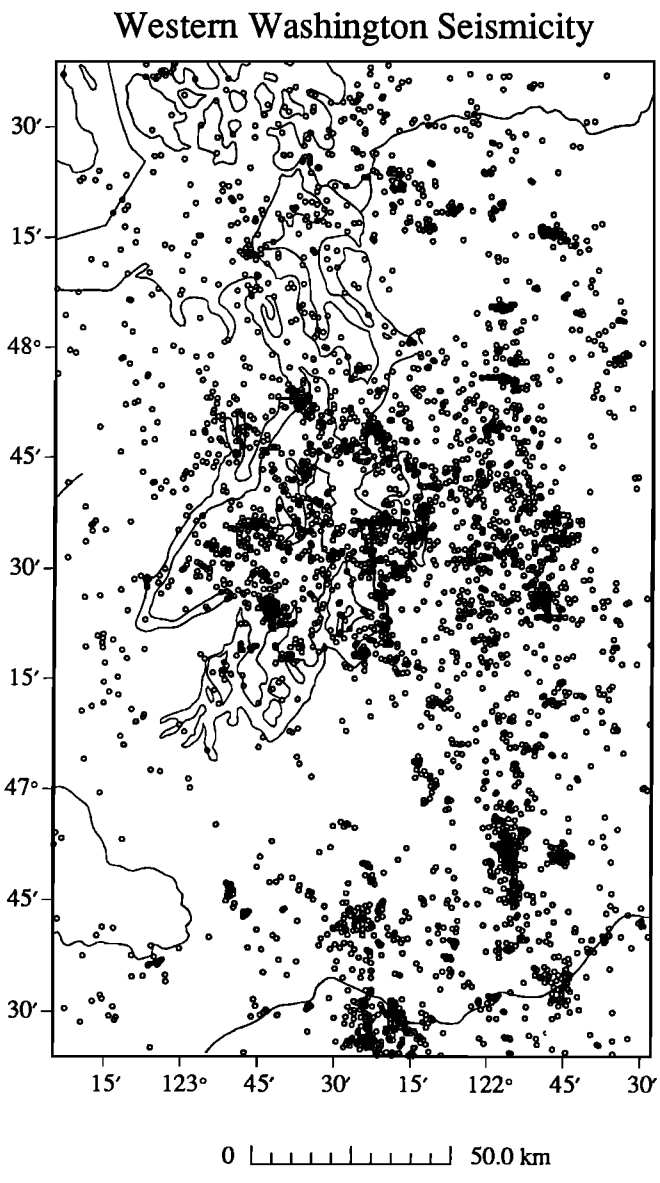

Fig. 2. Map of 4,387 earthquake epicenters used in the inversions.

Inversion Method

The method used to invert for P-wave velocity has been generally described by *Aki and Lee* [1976], *Aki et al.* [1977], *Thurber* [1983], *Humphreys and Clayton* [1988], and *Lees and Crosson* [1989] and others. The technique is briefly outlined as follows: A one-dimensional layered velocity model is derived by joint hypocenter-velocity model determination following *Crosson* [1976] using a small subset of high quality data. This model is used to locate the remaining earthquakes and station corrections are determined as discussed above. Raytracing is performed with respect to the model and the target volume is divided into small, nearly cubical blocks. Using A_{ij} to denote the matrix relating the length of the ith ray in the jth block, the relationship between the travel time residuals t and the slowness perturbations s can be formulated as a large sparse system of linear equations,

$$\mathbf{As} = \mathbf{t} \tag{1}$$

This system is overdetermined, inconsistent and underconstrained, and therefore requires some form of regularization to achieve a meaningful solution. We have adopted a method similar to the Levenberg-Marquardt approach except we augment the system using the discrete 2-dimensional Laplacian weighting operator in the horizontal plane [*Lees and Crosson*, 1989]. This leads to an augmented system of equations,

$$\begin{bmatrix} \mathbf{A} \\ \lambda \mathbf{L} \end{bmatrix} \mathbf{s} = \begin{bmatrix} \mathbf{t} \\ \mathbf{0} \end{bmatrix} \tag{2}$$

where L represents the Laplacian operator and λ is a scalar constant. Laplacian weighting is done independently for all horizontal planes. Since differentiation represented by the Laplacian is a roughening operation, constraining the Laplacian to be zero has the effect of a smoothing filter [*Crosson and Lees*, 1989].

Uncertainty in the arrival time of the signal is used to weight the equations of (2) by pre-multiplying A and t by

$$\mathbf{W} = \left[\frac{1}{s_1}, \frac{1}{s_2}, \ldots, \frac{1}{s_n} \right] \mathbf{I} \tag{3}$$

where s_i is the estimated uncertainty in the i-th observation. In addition to this weighting scheme, the biasing effects of large

clusters of rays can be attenuated by averaging rays that occur in respective ray clusters. This is achieved by weighting the equations associated with a ray cluster according to the number of rays that occur in the cluster. Thus each ray of a cluster has an additional weight applied to it equal to 1/k, where k is the number of rays in its associated cluster. These weights are incorporated into the W matrix. After this modification,we are left to solve

$$\begin{bmatrix} WA \\ \lambda L \end{bmatrix} s = \begin{bmatrix} Wt \\ 0 \end{bmatrix} \quad (4)$$

The least-squares solution of this system minimizes

$$\|WAs - Wt\|^2 + \lambda^2\|Ls\|^2 \quad (5)$$

where the parameter λ is used to adjust the relative weight of roughness versus misfit reduction as a trade-off parameter. To solve (4) we used the iterative, conjugate gradient technique (LSQR) of *Paige and Saunders* [1982]. The damping parameter λ = 1000 was chosen by trial and error such that a reasonable amount of misfit reduction and model smoothing was attained. After 30 iterations a 36% reduction in residual mean square error was achieved. A plot of the reduction in residual travel time is shown in Figure 3. It is clear that the majority of residual reduction is accomplished in the first 10 iterations (the

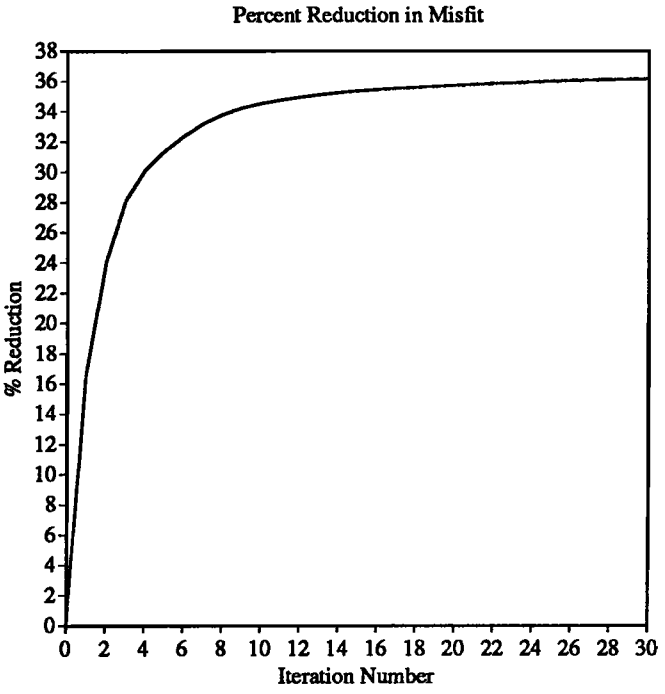

Fig. 3. Percent reduction of residual misfit versus iteration number. The inversion was done on Puget Sound data using the LSQR algorithm with regularization implemented by constraining the Laplacian to be zero in horizontal layers.

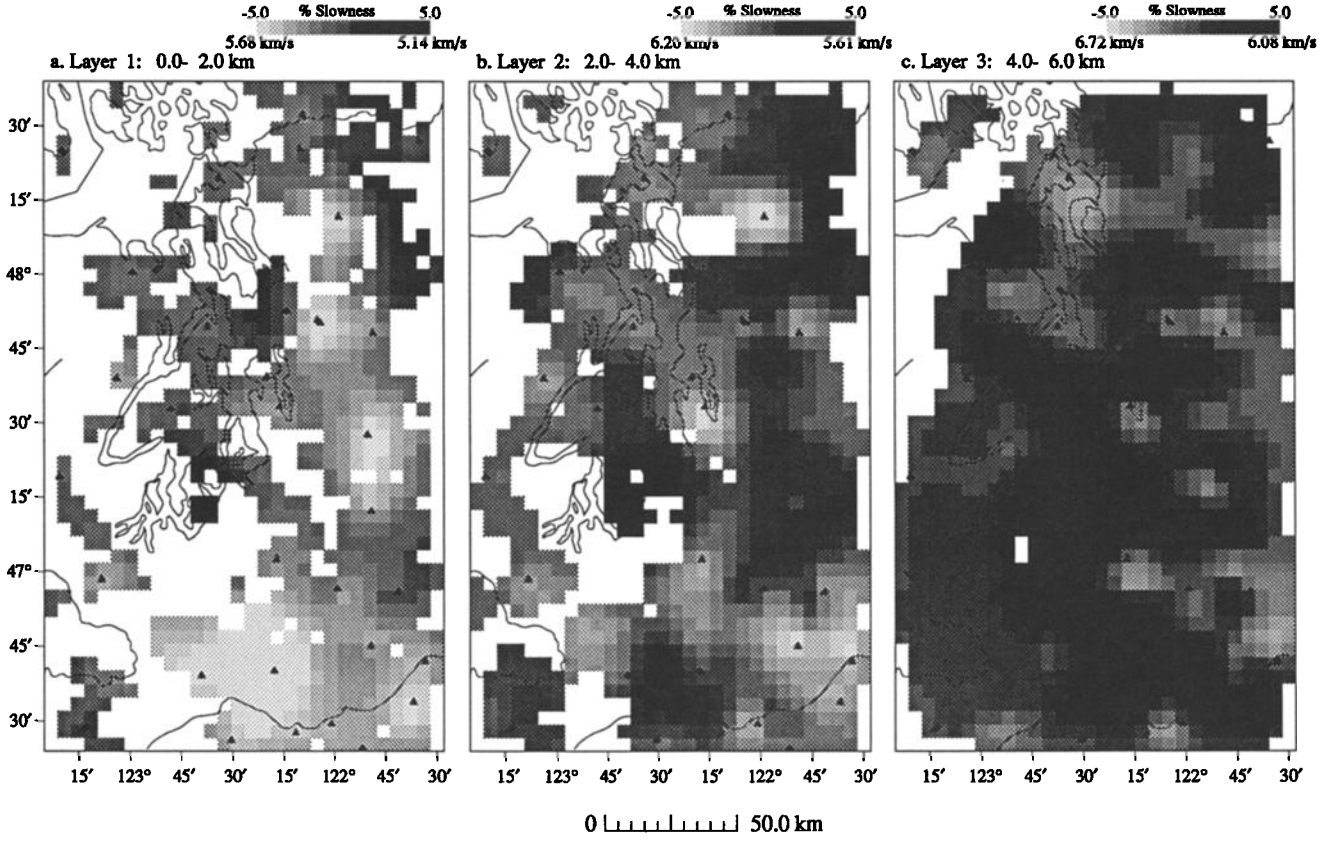

Fig. 4(*a-i*). Tomographic velocity inversion of the Puget Sound. Each Figure represents a horizontal slab in the earth. Grayshades represent ± 5.0 % slowness perturbations from the reference model and the corresponding absolute velocities are indicated beneath the scales. Light colored regions are high velocity and dark regions are low velocity. Dark triangles are station locations plotted for reference.

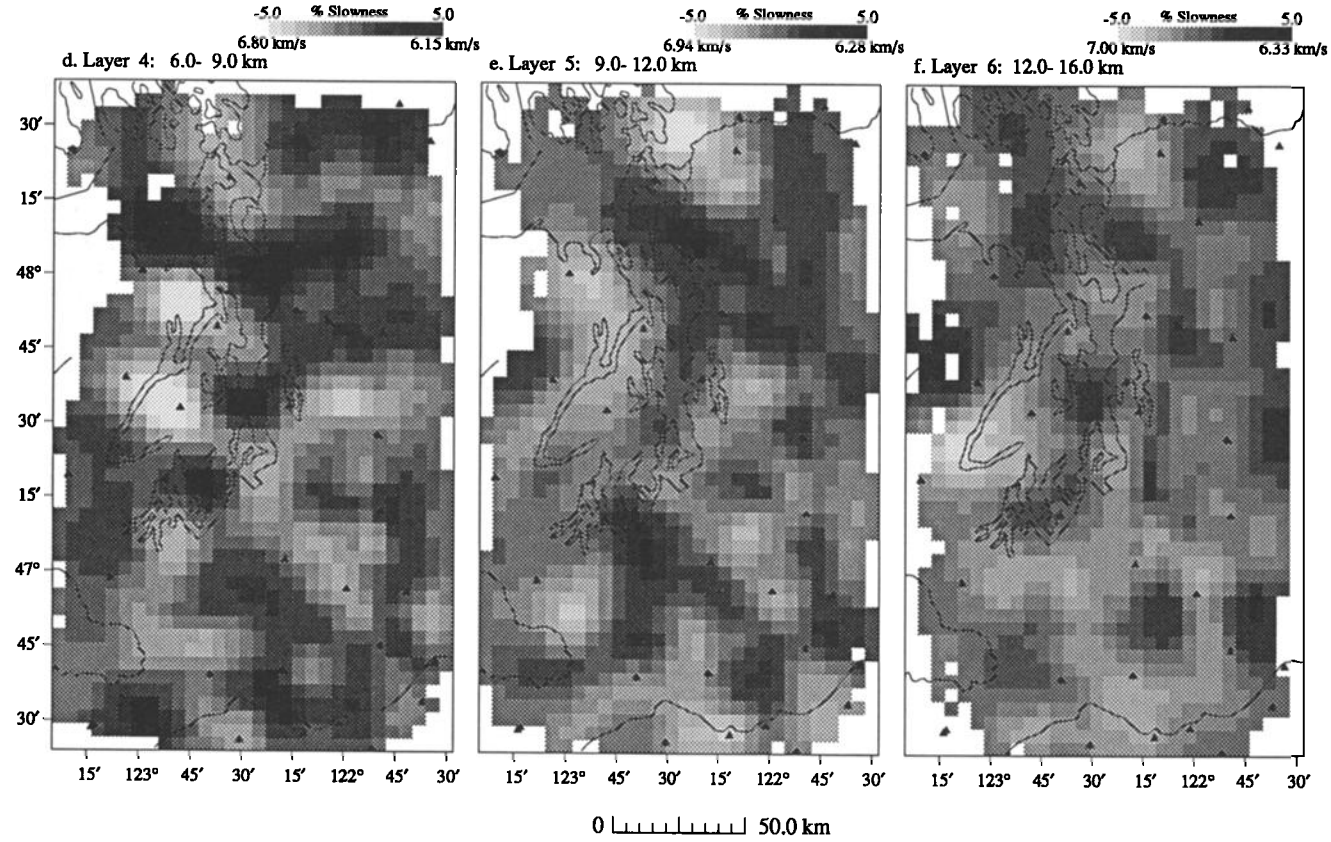

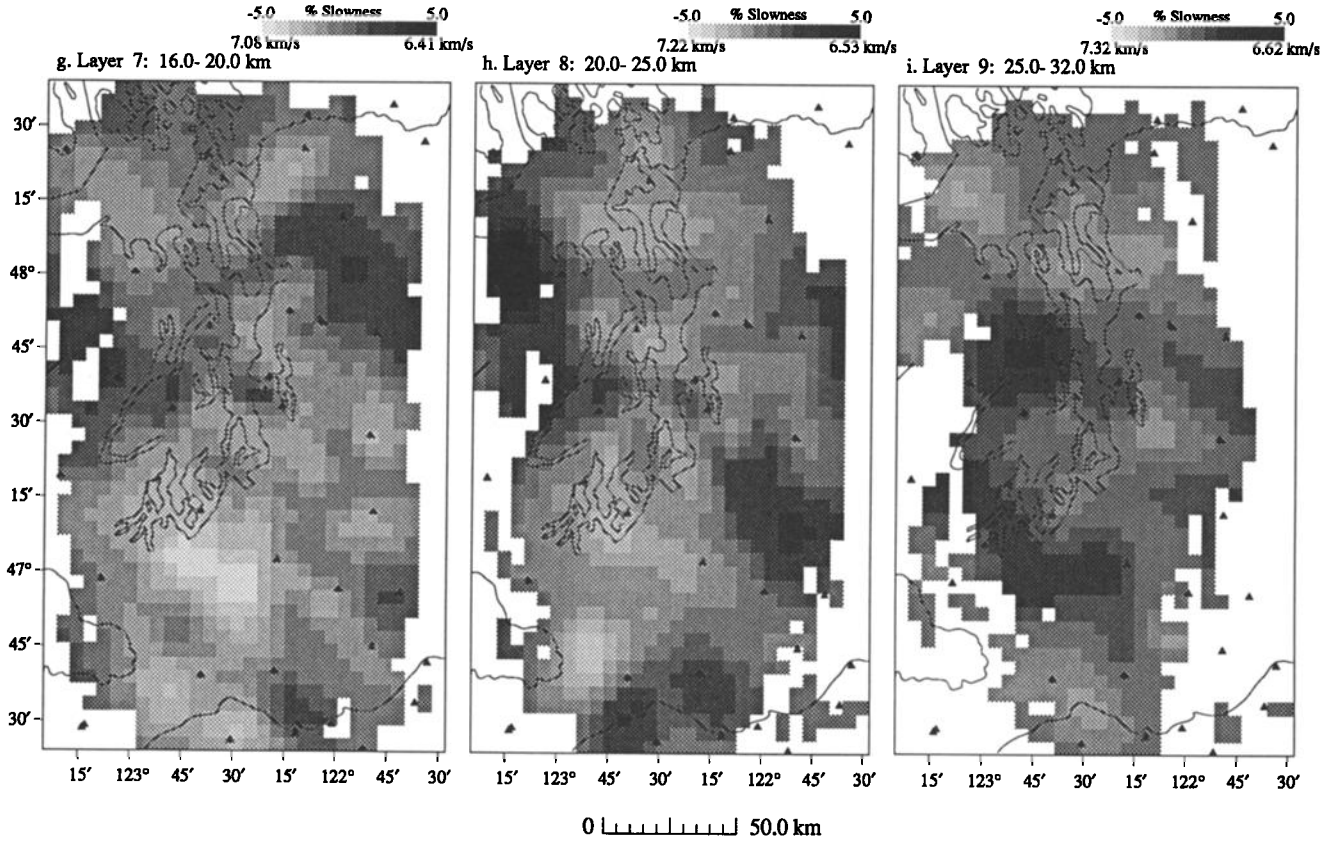

Fig. 4. (continued)

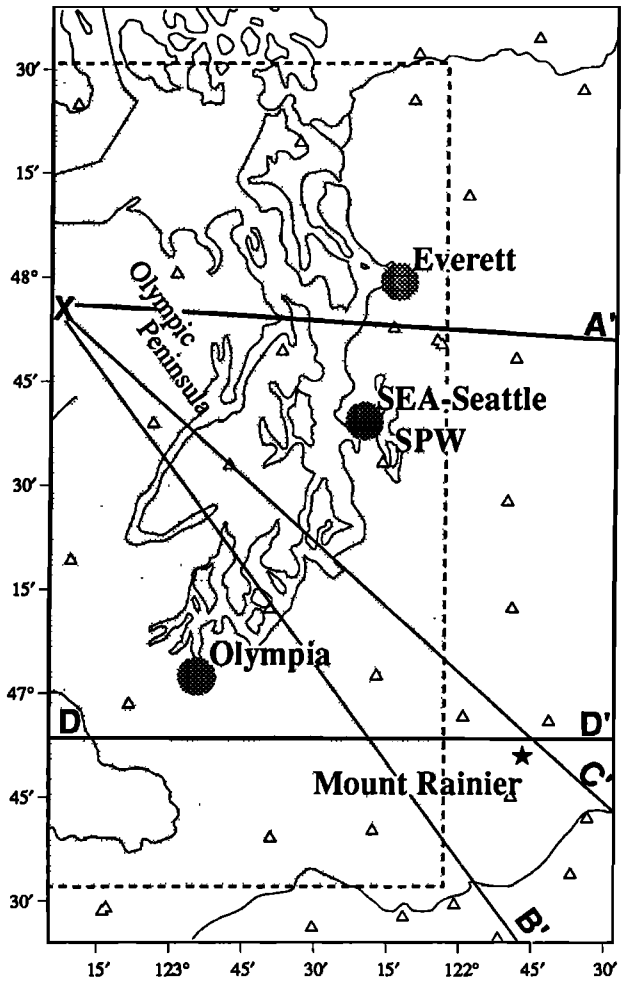

Fig. 5. Map of cross sections through model. The shaded area marks the outline of the gravity plot adapted from *Gower et al.* [1985], reproduced in Figure 9.

inversion took about 23 minutes of CPU time on a Ridge 32 mini-computer).

Inversion Results

To display results of the inversion, greyshade plots are provided for each layer individually (Figure 4a-i) and four vertical cross sections XA' to DD' (Figure 5) are displayed in Figure 6a-d. Since we have derived a three-dimensional perturbation model we prefer to display the results as perturbations from the background reference velocity, as opposed to absolute velocity values. In this way we remove the vertical structure, generally an increase with depth, which would otherwise dominate the image. The perturbations have been plotted with a common greyscale ranging from -5% to 5% slowness, however it should be noted that the actual perturbation ranges vary from layer to layer. The estimated extreme perturbation values and their respective absolute velocities for each layer are compiled in Table 1 for reference. The dark shades represent blocks whose slowness is anomalously high (low velocity) and lighter shades correspond to anomalously lower slowness (high velocity).

At the surface (1-2 km) a broad low, but rather weak, velocity anomaly is evident in the Puget Sound lowland, contrasting to the higher velocities situated to the east. This low velocity is more pronounced in the southern end of the Puget Basin where at 4-6 km depth it broadens and is large in amplitude (as high as 10% perturbation correponding to ~5.9 km/s). From 6-16 km this anomaly diminishes in extent and amplitude (3% perturbation). A northwest striking low velocity anomaly is apparent in the southern portion of the target beginning in layer 3 (4-6 km depth) and extending to the northeast to 12-16 km depth. This trend is apparent in layer 2 (2-4 km depth) as a high velocity anomaly. There are two low velocity anomalies, between 2-6 km depth, north of Seattle, at longitude 122°7.5' and latitudes 47°42' and 48° respectively. These may extend to 9 km depth but below layer 5 (9-12 km depth) there is little evidence of a continuation of this trend.

A high velocity anomaly is apparent in the western edge of the model beginning at 2-4 km depth beneath the present day exposure of the Crescent rocks in the Olympic Peninsula. This anomaly is most clearly observed between 6-12 km depths (6% anomaly, ~7.0 km/s) where it apparently extends east beneath the Puget Sound low. At 16-25 km the anomaly appears to broaden in lateral extent.

The eastern edge of the target is dominated by alternating high and low perturbations particularly evident between 2-12 km depths. In the Mount Rainier region low amplitude high velocity anomalies appear to flank the volcano to the east and the west to depths of 9 km. From 9-25 km depth there appears to be a low velocity anomaly beneath Mt. Rainier.

The northern portion of the target exhibits a high velocity anomaly beginning at 6 km depth which appears to be surrounded by a ring of lower velocity material. Between 16-32 km depth the anomalies generally appear to broaden, perhaps due to lower resolution at these depths. In layers 7-9 (16-32 km depth) a low velocity anomaly is observed on the western edge of the target that appears to dip eastward.

Resolution and Error

The resolution of the tomographic inversions presented here is primarily a function of the ray distribution and the smoothing imposed by regularization. (We chose block dimensions smaller than our expected resolution such that the a priori smoothing rather than block size would control the lateral resolution. Also, since the observations were recorded on short period instruments, signal wavelength was not a limiting factor for resolution. Ideally we desire the resolution kernel at every point in the model, but for inversions of this scale, where there are thousands of model parameters and tens of thousands of data, it is impractical to calculate the resolution matrix. Furthermore, even if we had the resolution matrix there is presently no convenient way of displaying all of the information in a manner that would be useful. The resolution for one block can be calculated by placing a unit spike in the block (i.e. slowness perturbation = 1), computing the forward travel times through the spike model and inverting the output as outlined above. The result is the impulse response (point spread function) of the system for that block. If the ray coverage in the vicinity of the block is homogeneous and isotropic, then the impulse response will be uniform and representative over the region [*Humphreys and Clayton*, 1988]. Resolution impulse responses used in conjunction with ray distribution descriptions can therefore be used as a

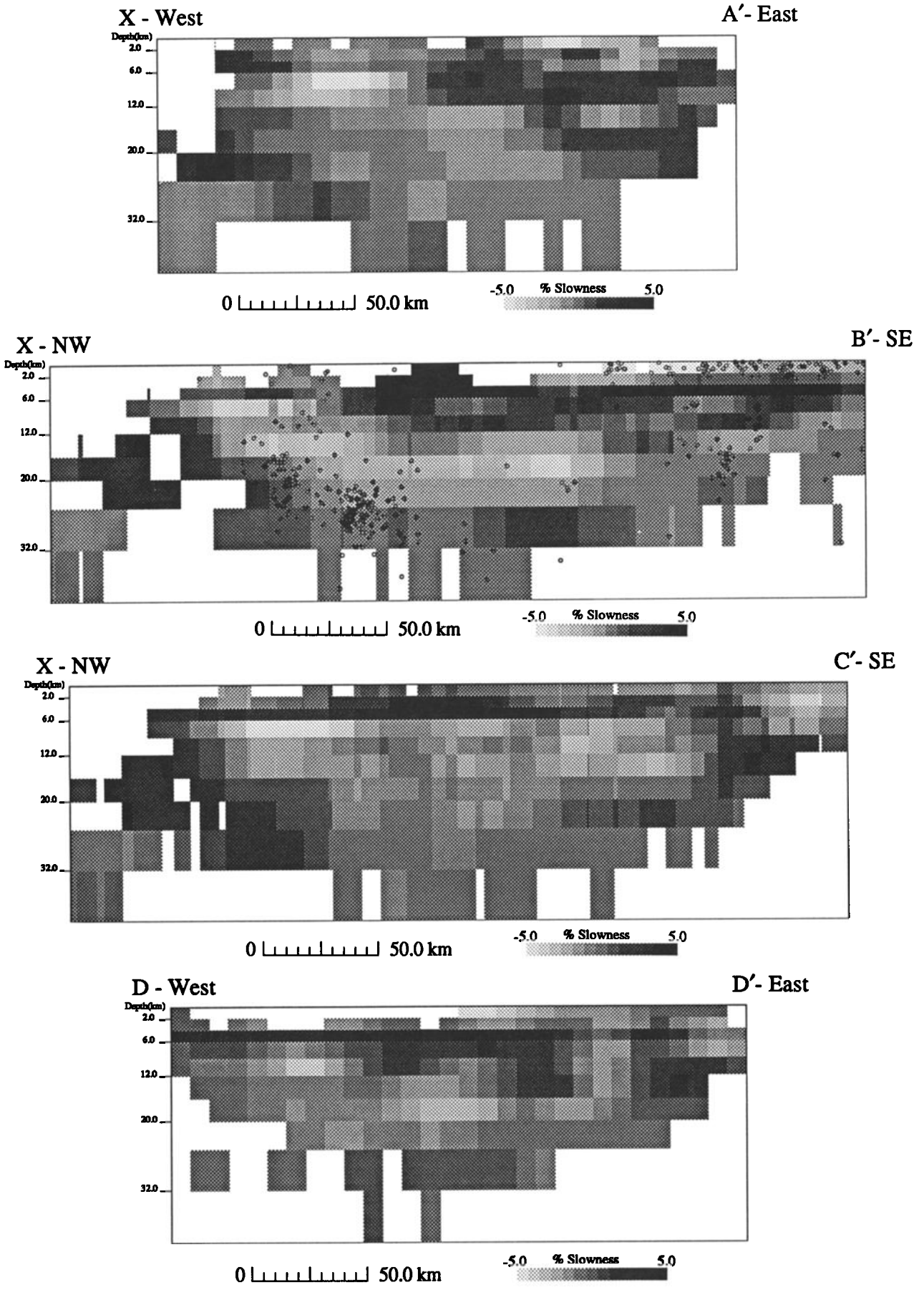

Fig. 6(*a-d*). Vertical cross sections through the Puget Sound Model. The 3-D model has been sliced along lines illustrated in Figure 5 and the layers are displayed with the common grayshade scale according to Figure 4. *a*) Cross section XA' crosses the Olympic Peninsula north of Seattle. *b*) The structure of the Crescent formation can be seen dipping to the southeast in section XB'. The seismicity in a 20 km swath has been projected on this cross section. *c*) Section XC' traverses northwest-southeast passing near Mt. Rainier. *d*) East-west cross section DD' corresponds to Transect B3 [*Cowan and Potter*, 1986].

qualitative substitute for the full resolution calculation in the case where the model parameters are very numerous. We have examined both simple descriptions of the ray coverage, such as hit-count displays, as well as more detailed descriptions such as the ray ellipsoid method [*Kissling et al.*, 1984; *Lees*, 1989]. In addition, we have also inspected the response of the system to various spatially regular test patterns [*Hearn and Clayton*, 1986; *Spakman and Nolet*, 1988]. For the most part, these techniques indicate that the resolution of our inversion is generally at a finer scale than the broad features we interpret in this study.

An example impulse response located in the vicinity of Mt. Rainier at a depth of 6-9 km is presented (Figure 7a-c). While the resolution here is not quite as good as in the center of the model, the resolution length is still in the range of 15-20 km (3-4 blocks). The amplitude of the central block of the impulse response is 12% of the original unit spike. There is smearing in the layers above and below this position as indicated by the side lobes in layers 3 and 5, although the amplitude of the side lobes is down by over 30% from the central block. At the surface and on the edges of the target volume there is more smearing in the vertical direction due to rays leaving and arriving at the end points of raypaths.

The standard errors are estimated using the jackknife [*Efron*, 1982; *Lees*, 1989; *Lees and Crosson*, 1989]. This method involves partitioning the data into subsets such that each partition excludes a different, non-overlapping portion of the data. Inversions are performed for each data partition and statistics (e.g. the standard error) are accumulated for each model parameter. In this study results of the jackknife with 30 partitions are presented in Figure 8. Overall the errors are relatively small, less than 2.7% over the whole model. In layer 3 (4-6 km) there is a high estimated standard error (2.7%) near the center of the target. The dominant anomaly in this region is approximately 8.2% so the ±2.7% is not large enough to wipe the anomaly out, i.e. the sign of the anomaly is well constrained. This is true for all the blocks that have high ray coverage density over them. This indicates that random errors inherent in the data, due to misspicking or mislocation, do not introduce large spurious anomalies into the model.

DISCUSSION

Both gross features of the surface geology and several details surmised from independent geophysical studies are consistent with the anomalous velocity structures imaged by the seismic tomography. Three large low velocity anomalies appear in the central and southern Puget Sound regions which correlate well with large gravity anomalies in this area [*Bonini et al.*, 1974]. A reproduction of the gravity contours for the central Puget Sound region is illustrated in Figure 9 and a close up of layer 3 is duplicated in Figure 10 for comparison. We interpret the low velocity anomalies of the central Puget Sound as deep sedimentary basins. *Gower et al.* [1985] interpreted the two prominent negative gravity anomalies north of SEA and Everett and the northwest trending lineation of the southern Puget Sound region to be primarily fault controlled. The southern anomaly prominent in layer 3 (4-6 km depth) appears to correlate well with a high aeromagnetic anomaly observed by *Stanley et al.* [1987]. These features appear in the three-

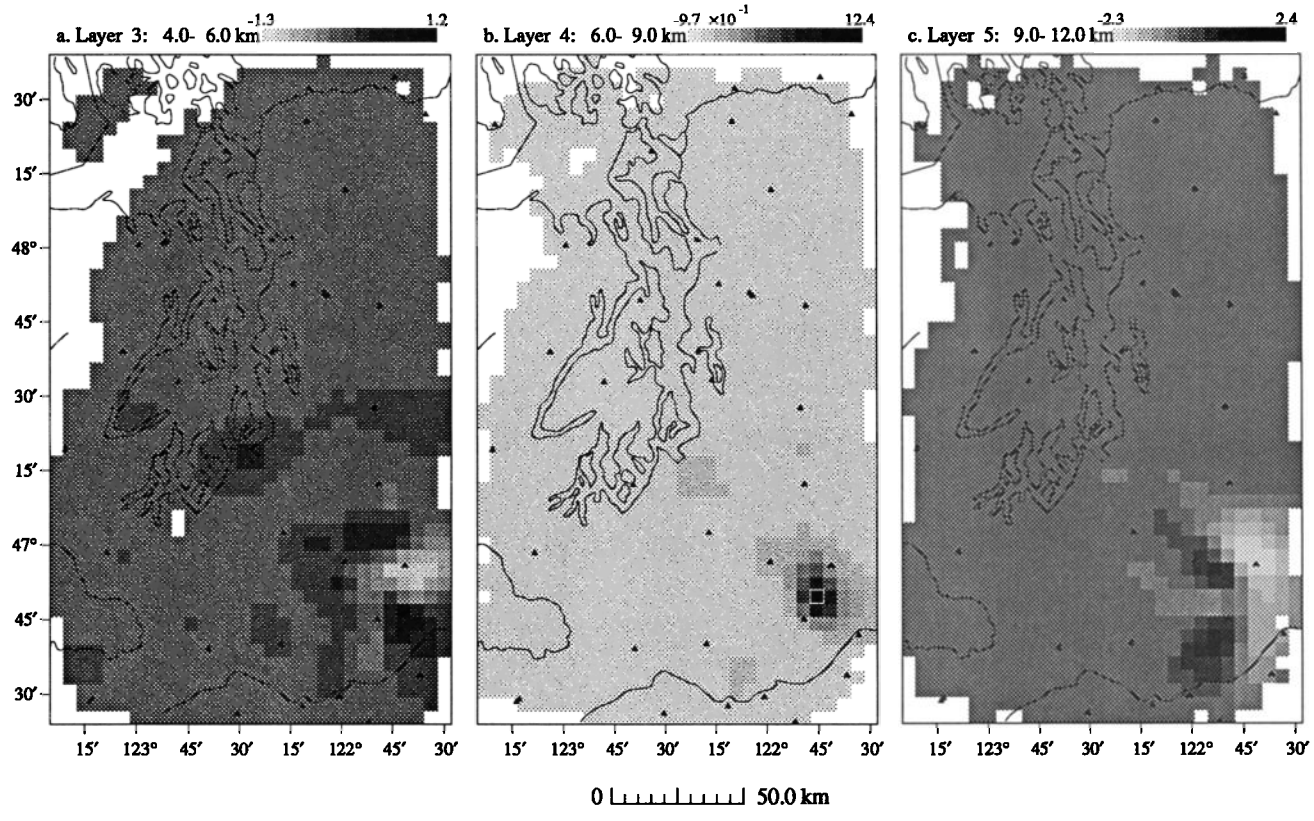

Figure 7

Fig. 7(*a-c*). Resolution kernel located near Mt. Rainier in layer 4, depth 6-9 km. The lateral resolution in this area is approximately 3 blocks, or 15 km. While there is smearing in the vertical direction the amplitude of the side lobes is down by a third of its value in layer 4..

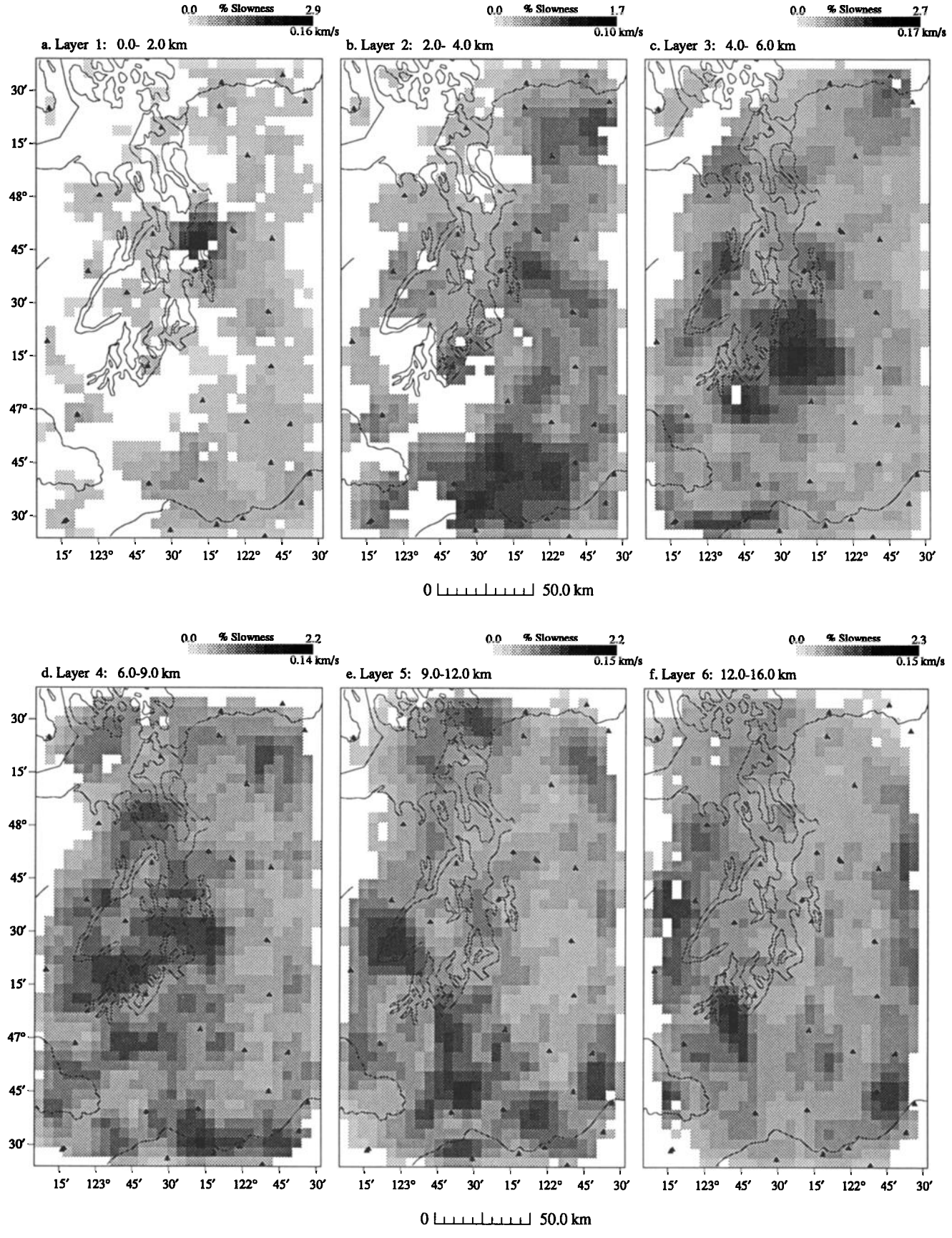

Fig. 8. Jackknife estimates of the standard errors for the Puget Sound inversion. The jackknife was applied using 30 partitions of the data, each inverted with the LSQR algorithm with the Laplacian constrained to zero for regularization. Error assessment should be used in conjunction with resolution estimation for overall determination of the uncertainties in the inversion results.

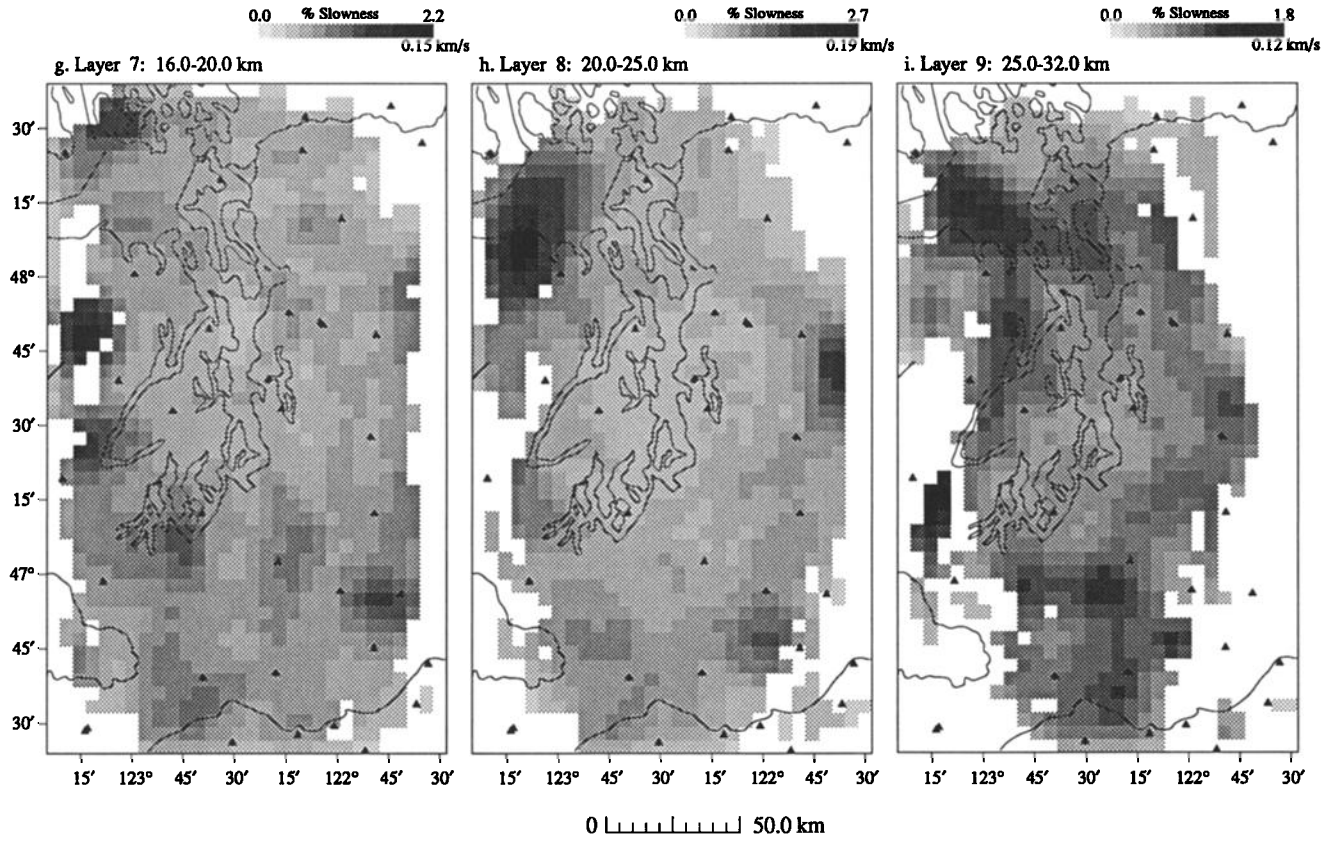

Fig. 8. (continued)

dimensional model as low velocity perturbations perhaps indicating rocks of sedimentary origin. The high correlation of gravity and slowness perturbation images suggests that gravity could be used to constrain seismic velocity inversion [*Lees and Vandecar*, 1989].

The Crescent rocks on the eastern flank of the Olympics appear in our model as a high velocity anomaly, contrasting with the sedimentary deposits in the Puget Sound lowlands. Since the low velocity anomalies west of the Puget Sound lowlands, between 16-32 km depths, are on the edge of the model, where resolution is poor, we can only speculate that these anomalies represent the sedimentary core rocks emplaced beneath the Crescent basalts. East-west vertical cross sections through the model (Figures 5, 6 and 11) suggest that the Crescent rocks dip to the east with an apparent dip of 18-28°. The dip inferred from the model is comparable with results from the Lithoprobe experiments near southern Vancouver Island [*Clowes et al.*, 1987]. At 9-12 km depth the velocity of this anomaly is approximately 6.8±0.07 km/s compared to the *Taber* [1983] estimate of 6.7 km/s at 10 km depth for this area. We do not have as much confidence in the absolute values of the velocities as our error analysis might suggest, however they are not entirely unreasonable for buried basalts. The Crescent anomaly appears to broaden laterally at depths of 16-25 km primarily in the southern Puget Sound region. If the high velocity anomalies at depths of 10-20 km below the southern Puget Sound represent an accumulation of dense, competent Crescent rocks, then this may provide an explanation for the lack of seismicity (Figure 2) in the southwest quadrant of our study area compared to the extensive seismicity north of latitude 47°15'.

In the vicinity of Mount Rainier small, shallow, higher velocity structures appear to correlate with plutons observed at the surface [e.g. *Walsh et al.*, 1987]. Cross section DD' suggests evidence for buried plutonic structures flanking Mount Rainier inferred by *Cowan and Potter* [1986]. These structures resemble similar features found by Lees and Crosson [1989] in the vicinity of Mount St. Helens. A large low velocity anomaly is evident below Mt. Rainier, generally corresponding to the large gradients in conductivity interpreted by *Stanley et al.* [1987].

The eastern and northern regions of the model are complicated by alternating high and low velocity anomalies. We believe this reflects the corresponding complex geological structure of this region where pre-Tertiary sedimentary and volcanic rocks have been accreted to the North American plate. In the eastern portion of the study region, the presence of many rather localized high velocity anomalies (e.g. 4-6 km depth range) could represent plutonic bodies that are not apparent at the surface.

CONCLUSIONS

The broad scale features of the three-dimensional tomographic inversion appear to correlate well with many known surface geologic features as well as some independent geophysical measurements. These correlations indicate that the velocity structures derived using the tomographic method

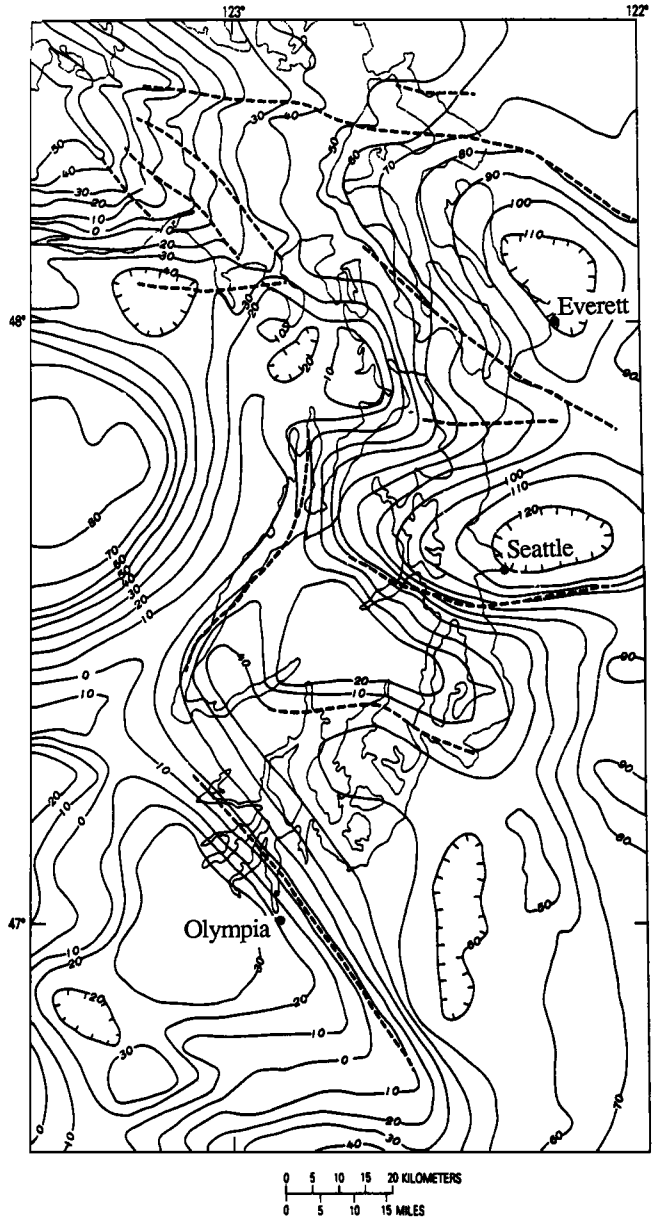

Fig. 9. Regional Bouguer gravity map in milligals. Dashed lines represent inferred faults from gravity and seismicity studies as described by *Gower et al.* 1985]. The geographical bounds of this plot are illustrated in Figure 5.

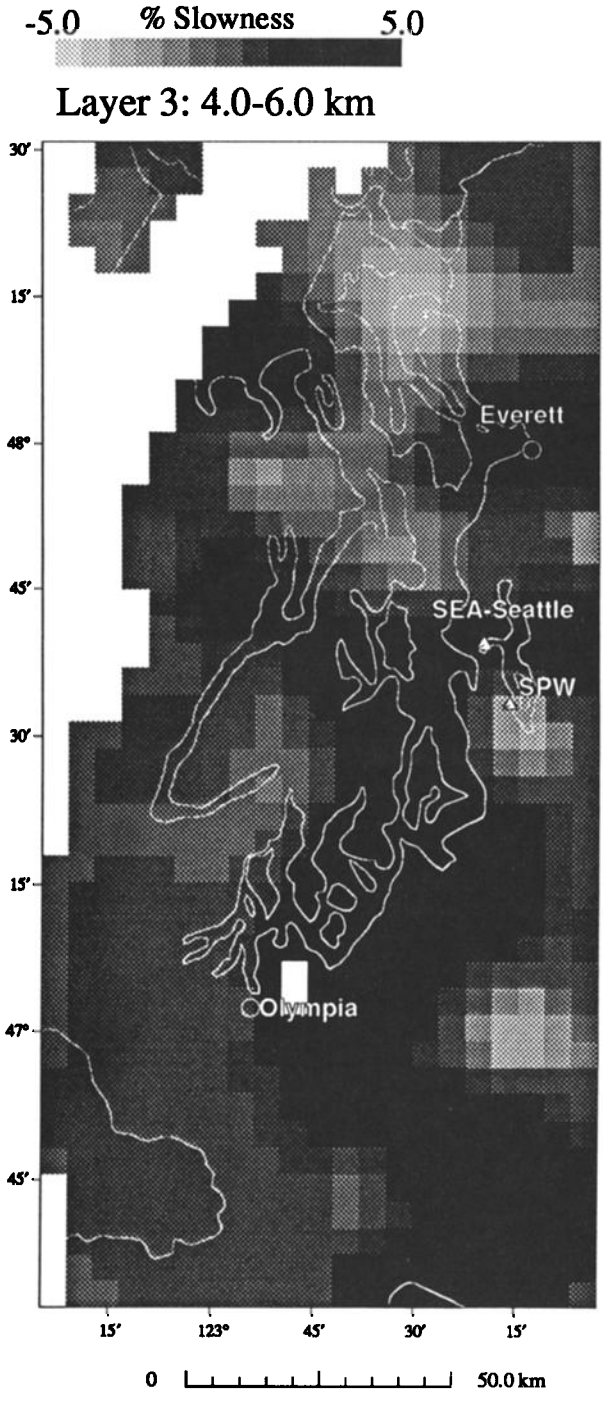

Fig. 10. Close-up of Layer 3 from Figure 4. To compare velocity structure to Bouguer gravity structures, this is plotted at same scale as Figure 9 and has been cropped approximately to the same area as shaded in Figure 5.

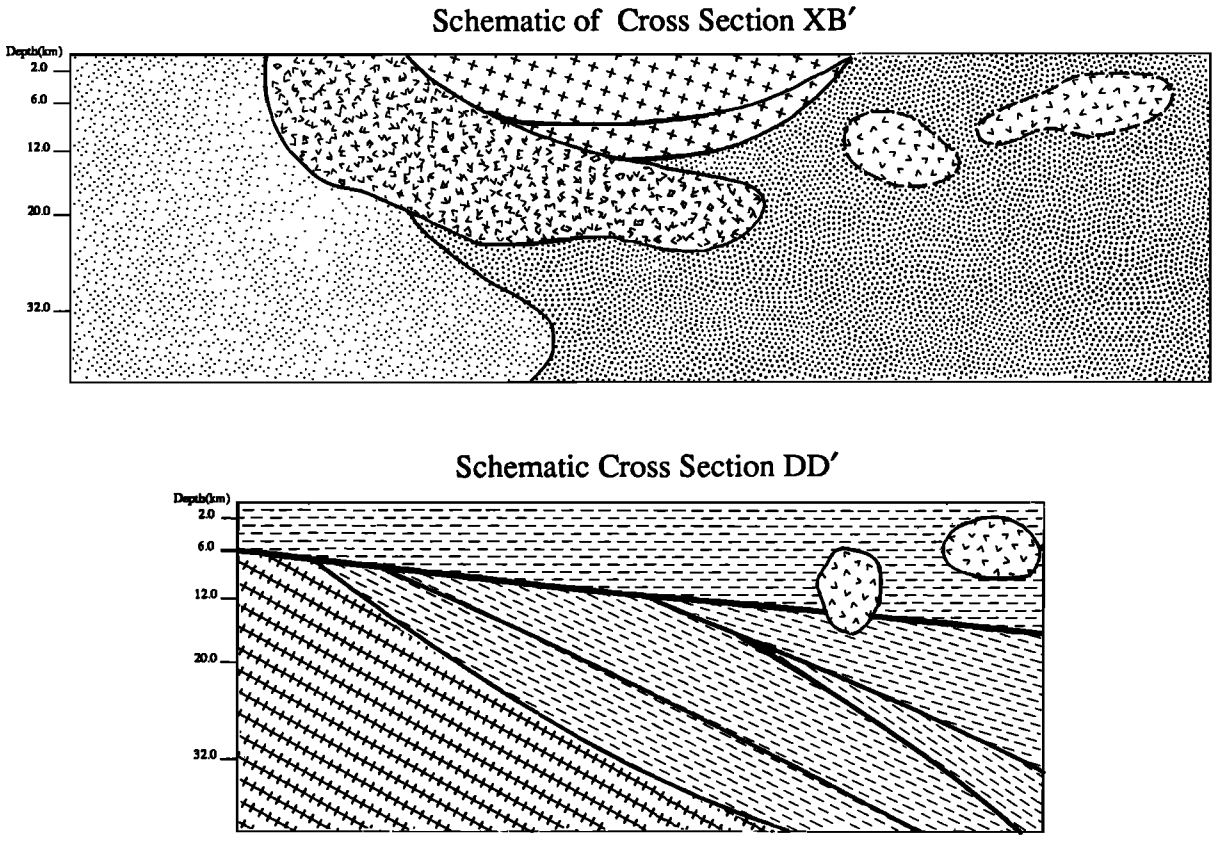

Fig. 11. Schematic plots illustrating interpreted features along cross sections of Figure 6. *a*) Interpretation of section XB' showing the Crescent basalts dipping below the Puget Sound sediments and possible location of buried plutons. The boundary below the basalts is meant to distinguish rocks west and east of the Puget Sound. *b*) Schematic interpretation of section DD' partially adapted from *Cowan and Potter*'s [1986] Transect B3.

indeed reflect important geologic structures in the subsurface. In particular we have imaged a deep sedimentary basin below the southern Puget Sound lowlands and two basins north of Seattle. The Crescent formation is represented by a high velocity anomaly which apparently dips eastward beneath the Puget Sound. In the vicinity of Mount Rainier several higher velocity structures appear to correlate with exposed and buried plutons.

Acknowledgements. The authors are grateful to Craig Weaver and Darrel Cowan for many helpful discussions. Donna Eberhart-Phillips and one anonymous reviewer contributed helpful suggestions to improve the manuscript. Linda Myerson helped draft several of the figures. This work was supported by USGS grants 14-08-0001-G1080 and 14-08-0001-G1390.

REFERENCES

Aki K., and W. H. K. Lee. Determination of three dimensional velocity anomalies under a seismic array using first P arrivals from local earthquakes. *J. Geophys. Res., 81*, 4381-4399, 1976.

Aki, K., A. Christoffersson, and E. S. Husebye, Determination of the three-dimensional seismic structure of the lithosphere, *J. Geophys. Res., 82*, 277-296, 1977.

Armstrong, R. L., Cenozoic igneous history of the U.S. Cordillera from latitude 42° to 49° north, in *Cenozoic tectonics and regional geophysics of the western Cordillera*, pp. 265-282, Geol. Soc. Am., 1978.

Atwater, T., Implications of plate tectonics for the Cenozoic tectonic evolution of western North America, *Geol. Soc. Am. Bull., 81*, 3513-3536, 1970.

Bonini, W. E., D. W. Hughes, and Z. F. Danes, Complete Bouguer gravity anomaly map of Washington, *Gravity Anomaly Map GM-11*, Washington Division of Geology and Earth Resources, scale 1:500,000, 1974.

Clowes, R. M., M. T. Brandon, A. G. Green, C. J. Yorath, A. S. Sutherland, E. R. Kanesewich, and C. Spencer, LITHOPROBE-southern Vancouver Island: Cenozoic subduction complex imaged by deep seismic reflections, *Can. J. Earth Sci., 24*, 31-51, 1987.

Cowan, D. S. and C. J. Potter, Continent-ocean transect B3: Juan De Fuca spreading ridge to Montana thrust belt, Geol. Soc. Am., Boulder, CO., 1986.

Crosson, R. S., Crustal structure modeling of earthquake data 1. Simultaneous least squares estimation of hypocenter and velocity parameters, *J. Geophys. Res., 81*(17), 3036-3046, 1976.

Crosson, R. S., and J. M. Lees, Regularization or smoothing in inversion and seismic tomography as a linear filtering operation, *Eos Trans. AGU, 70*(20), 601, 1989.

Crosson, R. S. and T. J. Owens, Slab geometry of the Cascadia subduction zone beneath Washington from earthquake hypocenters and teleseismic converted waves, *Geophys. Res. Lett., 14*, 824-827, 1987.

Duncan, R. A., A captured island chain in the Coast Range of Oregon and Washington, *J. Geophys. Res., 87*(B13), 10,827-10,837, 1982.

Efron, B., *The Jackknife, the Bootstrap and Other Resampling Plans*, Society for Ind. and Applied Mathematics, Philadelphia, Pa., 1982.

Evarts, R. C., R. P. Ashley and J. G. Smith, Geology of the Mount St. Helens area: Record of discontinuous volcanic and plutonic activity in the Cascade Arc of southern Washington, *J. Geophys. Res., 92*, 10,155-10,169, 1987.

Finn, C., and D. L. Williams, An aeromagnetic study of Mount St. Helens, *J. Geophys. Res.*, *92*, 10,194-10,206, 1987.

Gower, H. D., J. C. Yount and R. S. Crosson, Seismotectonic map of the Puget Sound region, Washington, *Misc. Invest. Map I-1613*, U.S. Geol. Surv., 1985.

Hall, J. B. and K. L. Othberg, Thickness of unconsolidated sediments, Puget Lowland, Washington, *Geologic Map GM-12*, Washington Division of Geology and Earth Resources, 1:316,800, 1974.

Hearn, T. M. and R. W. Clayton, Lateral velocity variations in southern California. 1. Results for the upper crust from Pg waves. *Bull. Seismol. Soc. Am.*, *76*(2), 495-427, 1986.

Humphreys, E. and R. W. Clayton, Adaptation of back projection tomography to seismic travel time problems, *J. Geophys. Res.*, *93*, 1073-1085, 1988.

Ishida, M. and A. H. Hasemi, Three-dimensional fine velocity structure and hypocentral distribution of earthquakes beneath the Kanto-Tokai district, Japan, *J. Geophys. Res.*, *93*(B3), 2076-2094, 1988.

Johnson, S. Y., Evidence for a margin-truncating transcurrent fault (pre-late Eocene) in western Washington, *Geology*, *12*, 538-541, 1984.

Kissling, E., W. L. Ellsworth, and R.S. Cockerham, Three-dimensional structure of the Long Valley Caldera, California, region by geotomography, Proc. of Workshop XIX, Active tectonic and Magmatic Processes beneath Long Valley Caldera, Eastern California, 1, *U.S. Geol. Surv. Open File Report 84-939*, 188-220, 1984.

Lees, J. M. and R. S. Crosson, Tomographic inversion for three-dimensional velocity structure at Mount St. Helens using earthquake data, *J. Geophys. Res.*, *94*(B5), 5716-5728, 1989.

Lees, J. M. and J. C. Vandecar, Seismic tomography constrained by Bouguer gravity anomalies, *Seism. Res. Lett.*, *60*(1), 11, 1989.

Lees, J. M., *Seismic Tomography in Western Washington*, Ph.D. Thesis, 173 pp., University of Washington, Seattle, 1989.

Manson, C. J., *Index to geologic and geophysical mapping of Washington, 1899-1983*, Washington Division of Geology and Earth Resources, 1984.

MacQueen, J. D., *Linear inversion of gravity data with geological and geophysical constraints*, Ph.D. Thesis, University of Washington, Seattle, 137 pp., 1982.

McBirney, A. R., Volcanic evolution of the Cascade Range, *Annu. Rev. Earth Planet. Sci.*, *6*, 437-456, 1978.

Paige, C. C. and M. A. Saunders, LSQR: An algorithm for sparse linear equations and sparse least squares, *Trans. Math. Software*, *8*, 43-71, 1982.

Spakman, W., and G. Nolet, Imaging algorithms, accuracy and resolution in delay time tomography, in *Mathematical Geophysics*, pp. 155-187, D. Reidel Publishing Co., 1988.

Stanley, W. D., C. Finn, and J. L. Plesha, Tectonics and conductivity structures in he southern Washington Cascades, *J. Geophys. Res.*, *92*, 10,179-10,193, 1987.

Taber, J. J., *Crustal structure and seismicity of the Washington continental margin*, Ph.D. Thesis, pp. 159, University of Washington, Seattle, 1983.

Taber, J. J., and B. T. R. Lewis, Crustal structure of the Washington continental Margin from refraction data, *Bull. Seismol. Soc. Am.*, *76*, 1011-1024, 1986.

Taber, J. J., and S. W. Smith, Seismicity and focal mechanisms associated with the subduction of the Juan de Fuca plate neneath the Olympic Peninsula, Washington, *Bull. Seismol. Soc. Am.*, *75*, 237-250, 1985.

Tabor, R. W., and W. M. Cady, Geologic map of the Olympic Peninsula, scale 1:125,000, *Misc. Invest. Map I-994*, U.S. Geol. Surv., Reston, Va., 1978.

Thurber, C. H., Earthquake locations and three-dimensional crustal structure in the Coyote Lake area, central California, *J. Geophys. Res.*, *88*(B10), 8226-8236, 1983.

Walsh, T. J., M. A. Korosec, W.M. Phillips, R.L. Logan, and H.W. Schasse, Geologic map of Washington - southwest quadrant, *Geologic Map GM-34*, Washington Division of Geology and Earth Resources , 1987.

Weaver, C. S. and S. W. Smith, Regional tectonic and earthquake hazard implications of a crustal fault zone in southwestern Washington, *J. Geophys. Res.*, *88*(B12), 10,371-10,383, 1983.

Wells, R. E., D. C. Engebretson, P. D. Snavely, and R. S. Coe, Cenozoic plate motions and the volcano-tectonic evolution of western Oregon and Washington, *Tectonics*, *3*, 275-294, 1984.

R. S. Crosson, University of Washington, Geophysics Program AK-50, Seattle, WA, 98195.

J. M. Lees, Institute for Crustal Studies, University of California, Santa Barbara, CA, 93106.

(Received May 16, 1989;
revised December 14, 1989;
accepted January 21, 1990.)